Annihilation mechanism of excitons in a MoS₂ monolayer through direct Förster-type energy transfer and multistep diffusion

Kwang Jin Lee [1], Wei Xin,[2] and Chunlei Guo [1,2,*]

[1]*The Institute of Optics, University of Rochester, Rochester, New York 14627, USA*
[2]*GPL, Changchun Institute of Optics, Fine Mechanics and Physics, Chinese Academy of Sciences, Changchun 130033, China*

An atomically thin MoS₂ layer is a direct bandgap semiconductor exhibiting strong electron-hole interaction due to the extreme quantum confinement and reduced screening of Coulomb interactions, which results in the formation of stable excitons at room temperature. Therefore, various excitonic properties of the MoS₂ monolayer are extremely important in determining the strength of light-matter interactions including their radiative recombination lifetime and optoelectronic response. In this paper, we report a comprehensive study of the underlying annihilation mechanism of various types of exciton in the MoS₂ monolayer using the transient absorption spectroscopy. We rigorously demonstrate that the Förster-type resonance energy transfer is the main annihilation mechanism of A and B excitons, while the multistep diffusion process is responsible for C-exciton annihilation, which is supported by critical scientific evidence.

I. INTRODUCTION

Two-dimensional (2D) transition metal dichalcogenides (TMDs) have emerged as fascinating materials for low-dimensional applications owing to their remarkable electronic and optical properties [1–5]. These materials are highly attractive for fundamental studies of novel physical phenomena and for applications ranging from nanoelectronics and nanophotonics to sensing and advanced optoelectronic devices [5–8]. For example, their unique electronic band structure exhibits many remarkable characteristics, such as gate-tunable conductivity with relatively high mobility [9], strong photoresponse [10], and valley-selective optical excitation [11–15]. Based on these properties, interesting functional devices have been developed, including field-effect transistors [9,16–18], broadband photodetectors [19], light-harvesting devices [20], photosensor [21], chemical sensor [22], and valleytronics [23–25].

2D TMDs are 2D semiconductors with direct bandgap lying in the visible and near-IR range at the energetically degenerate K and K ($-K$) points of hexagonal Brillouin zones, enabling strong interactions of dipole transitions with light [26]. The quantum confinement effect and reduced dielectric screening lead to strong Coulomb interactions between electrons and holes, resulting in tightly bound excitons with large binding energy (0.2 ∼ 0.8 eV) [27–29]. Therefore, applications based on 2D TMDs can be achieved by systematically understanding the excitonic properties such as excitonic band structure, migration dynamics, and multiexcitonic states.

Monolayer molybdenum disulfide (MoS₂), one of the members of 2D TMD materials, is a direct bandgap semiconductor with strong photoluminescence [26,30]. The excitonic property in monolayer MoS₂ is mainly dependent on the valence-band splitting due to strong spin-orbit coupling, which leads to Coulomb-enhanced multiexciton excitations at the band edge (K and K’ points), so-called the A and B excitons. Hence, various excitonic properties of A and B excitons such as exciton-absorption bleaching, interexcitonic interaction, and broadening has been intensively studied [31–36]. In addition, due to the parallel bands in their density of states, the MoS₂ monolayer shows strong optical responses for excitation energies higher than bandgap [32,33]. This photoexcited exciton in the "band nesting" region, denoted as the C exciton, exhibits a fast intraband relaxation and a very slow indirect emission process arising from spontaneous charge-separation in the momentum space [34,35]. Hence, the C exciton is delocalized to overlap with the continuum states near the K ($-$K) point in the Brillouin zone, leading to completely different hot-carrier relaxation process compared with the band-edge excitons (A and B excitons) [35,36]. It can also result in a strong optical response in absorption spectrum as with band-edge excitons.

The excitonic properties in 2D TMDs are extremely important in determining the confinement-enhanced characteristics. For example, exciton migration dynamics in MoS₂ monolayer is of high relevance for applications such as light harvesting systems and light emitting devices [37,38]. At high excitation intensities, a many-body interaction where one exciton is annihilated by transferring its energy to another exciton, so-called exciton-exciton annihilation (EEA), can take place in 2D TMDs [39–44] and organic semiconductors [45–51]. EEA usually occurs when two excitons are sufficiently close to interact and to generate a single exciton with a higher energy. This indicates that EEA is the additional deactivation process of excitons via interaction of two of them and is known to

*Corresponding author: guo@optics.rochester.edu

strongly affect the performance of light-emitting diodes at high excitation densities. A critical step in the operation of solar cells and photodetectors is also highly associated with EEA. For instance, the exciton diffusion length, the distance over which an exciton can migrate before it decays within its lifetime, is one of the most important parameters to optimize the photocurrent, which is dictated by the EEA process. In this context, comprehensive understanding of exciton annihilation and the accurate determination of the exciton diffusion length is essential for the optimization of photovoltaic device structures. Therefore, EEA is a crucial phenomenon to figure out the underlying mechanism of exciton annihilation in 2D semiconductors, organic polymers, carbon nanotubes, and molecular optical switches.

In general, EEA takes place through two distinct mechanisms, a direct Förster-type resonance energy transfer (FRET) and multistep diffusion [47]. FRET occurs in a way that direct long-range energy transfer via dipole-dipole interaction gives rise to annihilation, which depends primarily on the overlap between the emission spectrum of the donor and the absorption spectrum of the acceptor. In case of two identical excitons, a spectral overlap means the energy overlap between the exciton emission and the excited state absorption (ESA, absorption from the exciton state to higher electronic states), resulting in annihilation step, $E_1 + E_1 \rightarrow E_n + E_0 \rightarrow E_1 + E_0$ where E_0 and E_1 are ground state and exciton state, respectively. E_n is the final state upon photoexcitation. The highly excited state E_n generated by FRET relaxes quickly to exciton state E_1, thereby quenching efficiently one exciton [46]. On the other hand, the diffusion process induces a continuous exciton annihilation through the multiple transfer steps between the exciton and the ground state [46,52]. Consequently, the diffusion model assumes that the excitons move like random walkers in many steps towards each other of the type $E_1 + E_0 \rightarrow E_0 + E_1$, until they annihilate via a short range interaction in a final step of the type $E_1 + E_1 \rightarrow E_n + E_0 \rightarrow E_1 + E_0$.

Recently, we have studied the control of exciton dynamics in MoS$_2$ through optical interplay with hyperbolic metamaterials [53]. The study found that the Förster radius and FRET efficiency were enhanced by nonlocal effect from hyperbolic metamaterials. However, a more comprehensive study is required to understand why FRET and diffusion processes are dominant annihilation mechanisms for A and C excitons, respectively. In this article, we fully identify and characterize the annihilation of A, B-, and C excitons in a MoS$_2$ monolayer by employing ultrafast transient absorption spectroscopy. We demonstrate that A and B excitons are predominantly governed by FRET process while the diffusion process entirely dictates the annihilation of the C exciton, which is corroborated by several critical evidences.

II. SAMPLE AND EXPERIMENTAL METHODS

The preparation of a single-layer MoS$_2$ on silicon substrate $\langle 100 \rangle$, $\approx$300 nm SiO$_2$) is based on the traditional chemical vapor deposition method (high temperature, Argon environment for 2.5 h). MoO$_3$ (99.99%, Aladdin) and S (99.99%, Alfa Aesar) powders were chosen as precursor materials. Perylene-3, 4, 9, 10-tetracarboxylic acid tetra potassium salt was also
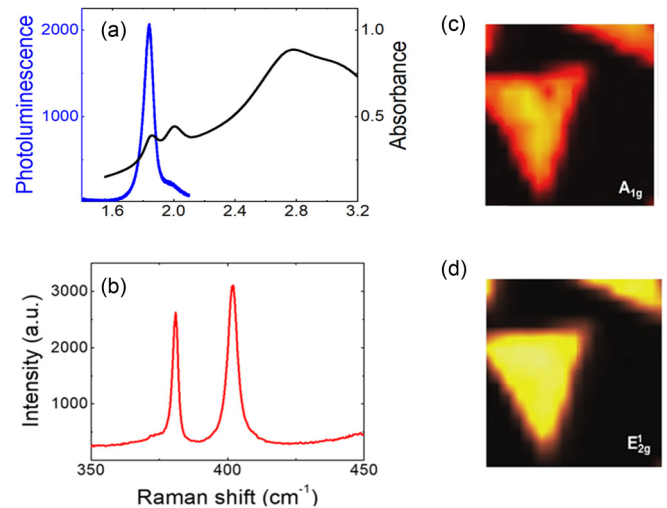

FIG. 1. (a) Absorption and photoluminescence spectra of MoS$_2$ monolayers. (b) Raman spectrum of MoS$_2$ monolayer (c) and (d), Raman intensity map for A_{1g} and E^1_{2g} modes, respectively.

dropped on the substrate as the seeding promoter to increase the nucleation. To remove the surface contaminants and make a close contact between MoS$_2$ and the substrate, annealing at 300 °C for 1 h was used. Figure 1(a) shows the absorption and photoluminescence spectra of MoS$_2$ monolayer. The two absorption peaks at 1.87 and 2.05 eV correspond to A and B excitons, respectively. The broad absorption band above 2.80 eV corresponds to the C excitons. The photoluminescence (PL) peak and shoulder at 1.84 and 2.01 eV are responsible for A and B excitons, respectively. No photoluminescence was observed for C excitons. The MoS$_2$ monolayer was characterized using Raman spectroscopy and displayed the expected Raman modes A_{1g} and E_{2g}, with $\sim$20 cm^{-1} separation for the monolayer area as shown in Fig. 1(b). Figures 1(c) and 1(d) display the Raman signal intensity map of the sample. We can clearly see the Raman signal for A_{1g} and E_{2g} modes at 382 and 402 cm^{-1}, respectively, which is consistent with the previous work [54].

To investigate the EEA, we employ ultrafast transient absorption (TA) spectroscopy based on the femtosecond pulse laser, which is incredibly useful tool to investigate the carrier dynamics, photosynthesis, and charge transfer dynamics in semiconducting materials [55–60]. All of the TA measurements were carried out at room temperature. A Ti:sapphire regenerative amplifier system operating at a repetition rate of 1 kHz and delivered 67-fs pulse duration centered at 800 nm was used. The laser output is split into a pump and a probe beam by a beam splitter. For the A and B excitons, the pump and probe beams were chosen by using a 5-mm-thick sapphire window for generating white-light-continuum, followed by band-pass filters centered at 2.25 eV for the pump and 1.85 eV (A exciton) and 2.01 eV (B exciton) for the probe. Probe beam energy was chosen by the PL peak energy of A and B excitons, 1.85 and 2.01 eV, respectively. For the C exciton, the second harmonic of the fundamental beam (using a BBO crystal) was chosen, which was further spilt into a pump and a probe. The pump beam was modulated using a mechanical

chopper at 220 Hz and the relative reflection $\Delta R/R$ of the probe beam as a function of the time delay was further read out with a photodiode. The relative reflectance is given by $\Delta R/R = (R_{on} - R_{off})/R_{off}$, where R_{on} and R_{off} are the sample reflectance with the pump beam on and off, respectively. In this study, we used linear polarized beam in the entire experiment, allowing us to rule out the valley-dependent effect. The effect of valley coherence on the EEA process by utilizing different optical helicity for pump and probe will be investigated in a future study.

III. THOERETICAL MODEL

In this section we discuss the EEA theoretically by considering exciton self-quenching dynamics. Typically, high excitation intensity or pump fluence is required to induce EEA, which may also induce other nonlinear phenomena such as Auger recombination. At higher excitation intensities, the exciton decay becomes more rapid at an initial time range but independent of the intensity at a longer time range. The faster decay strongly depends on the excitation intensity (or pump fluence), exhibiting higher order reactions resulting from EEA, while the slower decay corresponding to intrinsic exciton lifetime via the radiative and nonradiative deactivations process is independent of excitation intensity. TA kinetics for each exciton in the initial time range can be analyzed by the EEA formalism given by the rate equation as follows [47–49]:

$$\frac{d}{dt}n(t) = -\frac{n(t)}{\tau} - \frac{1}{2}\gamma(t)n(t)^2, \qquad (1)$$

where $n(t)$ is the exciton density at a delay time t, $\gamma(t)$ is the bimolecular annihilation rate coefficient proportional to $t^{-1/2}$, and τ is the intrinsic exciton lifetime at the low exciton density limit. The factor $1/2$ represents that only one exciton is left after EEA ($E_1 + E_1 \rightarrow E_n + E_0 \rightarrow E_1 + E_0 +$ phonon). In general, photoexcitation in conventional inorganic semiconductors such as III−V quantum wells generates free carriers, rather than excitons at room temperature. Therefore, the corresponding annihilation process can normally be described as a three-body Auger recombination process, a nonradiative decay mechanism commonly shown in highly excited semiconductors with free charge carriers. Indeed, exciton annihilation is generally analogous to the Auger recombination process. However, owing to the high exciton binding energy, biexcitonic interaction is dominant over the Auger process in monolayer MoS$_2$, and thus the Auger constant that is proportional to $n(t)^3$ can be neglected in this study [39]. Given that a typical III−V materials with band gap comparable to the A exciton energy in monolayer MoS$_2$ possess an extremely small Auger coefficient [61], many-body effects play a much more dramatic role in EEA processes in a MoS$_2$ monolayer than in conventional semiconductor systems [39]. Again, this difference is attributed to the strong confinement effects in the 2D nature and the associated reduced dielectric screening.

In Eq. (1), $\gamma(t)$ is given by Eqs. (2a) and (2b) for the FRET and diffusion models, respectively, as
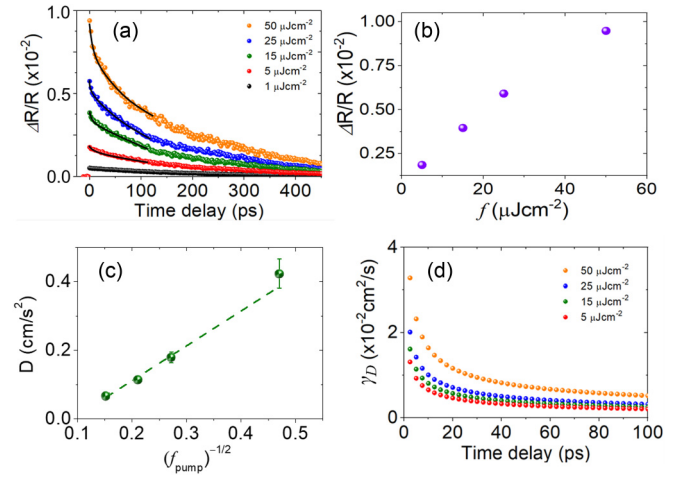

FIG. 2. (a) Transient absorption kinetics for the C exciton for pump fluences of 1, 5, 15, 25, and 50 μJ cm^{-2} with fitting (back) curves up to ∼100 ps based on exciton-exciton annihilation via diffusion [Eq. (3)]. (b) Initial amplitude of $\Delta R/R$ as a function of pump fluence. (c) Relationship between diffusion coefficient of C exciton exciton and inverse square root of pump fluence. (d) Plot of annihilation rate via diffusion as a function of time delay [Eq. (2a)].

follows:

$$\gamma_F(t) = \frac{R_F^2}{2}\sqrt{\frac{\pi^3}{\tau t}}, \qquad (2a)$$

$$\gamma_D(t) = \frac{1}{aN_0}\sqrt{\frac{8D}{\tau t}} \qquad (2b)$$

where R_F and D are the Förster radius and diffusion coefficient, respectively. a and N_0 are the lattice constant and molecular density, respectively.

IV. DIFFUSION PROCESS: C EXCITONS

As mentioned earlier, the parallel band region can promote self-separation of C excitons to generate hot carriers in momentum space, and they rapidly relax to nearest band extrema, the Λ and Γ valley. Recombination of these hot carriers from C excitons cannot generate photons owing to momentum mismatching, and they generally would release excess energy in the form of phonons. Because of this, even though the C exciton may not play a critical role in light-harvesting applications, comprehensive understanding C-exciton dynamics is essential to collecting the high-energy hot carriers [36].

Figure 2(a) shows the TA kinetics of C excitons in MoS$_2$ monolayer for different pump fluences ($f_{pump} = $ 1, 5, 15, 25, 50 μJ cm^{-2}) at 3.05 eV with probe energy of 3.05 eV. A positive signal of ΔR was attributed to a reduction of the available ground state carriers due to excitation from the pump, so-called a ground state bleach. Since the C excitons will not remain in a parallel band for a long time due to ultrafast self-separation, the photobleaching signals (amplitude of $\Delta R/R$) of the C exciton present a weaker signal compared to band-edge excitons (Fig. 3). However, weak TA signals of the C exciton cannot be influenced to acquire the decay dynamics of the C exciton. At the lowest f_{pump}, TA
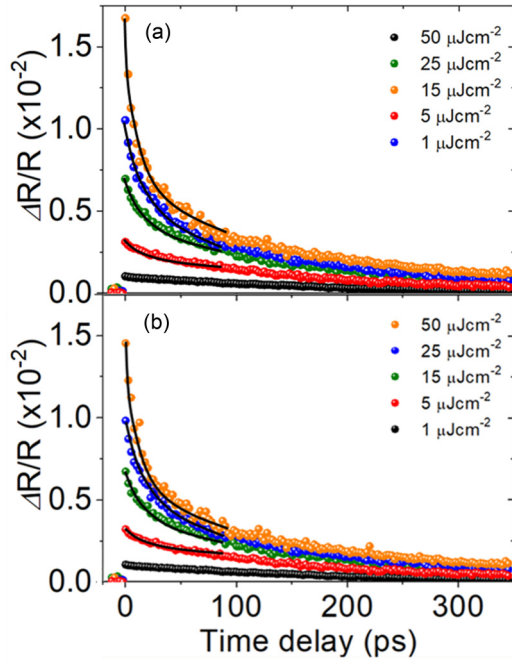
FIG. 3. (a) Transient absorption kinetics for the A exciton and (b) B exciton for pump fluences of 1, 5, 15, 25, and $50\,\mu J\,cm^{-2}$ with fitting (back) curves up to ~ 100 ps based on exciton-exciton annihilation via FRET [Eq. (4)].

kinetics show a single decay time (τ) of 219 ps, which corresponds to the intrinsic exciton lifetimes. As f_{pump} increases, an additional decay channel of the C exciton caused by EEA comes into play and leads to another shorter decay time constant formed in the initial delay time range (up to ~ 100 ps). We find that the short time constant (τ_1) decreases with f_{pump} while the intrinsic exciton lifetime (τ_2) is independent of f_{pump} (Table I). We note that τ_1 is responsible for EEA. Figure 2(b) exhibits the linear relationship between initial magnitude of the TA signal ($\Delta R/R$) and f_{pump}. Typically, at higher excitation levels, the bleach of the absorption band can also contribute to the TA signal, resulting in a $\Delta R/R$ that is no longer linear with f_{pump}. In this work, excitation intensities are all controlled to be in the linear region. For C excitons, FRET can be completely ruled out owing to their nonemissive property [52]. In order to determine the diffusion coefficient D, TA kinetics can be fitted by the solution of Eq. (1) for 1D

diffusion, which is given by [47,52,53]

$$n_{1D}(t) = \frac{n_0 e^{-t/\tau}}{1 + \frac{n_0}{aN_0}\sqrt{2D\tau}\,\mathrm{erf}\left(\sqrt{\frac{t}{\tau}}\right)}, \qquad (3)$$

where erf is the error function. n_0 is the initial exciton density right after photoexcitation determined by the relation $n_0 = f_{pump}(1 - 10^{-A})/E_{pump}$, where A and E_{pump} are the absorption coefficient and energy of pump beam, respectively. Here, the exciton lifetime τ was kept as a constant (213 ps). Black solid lines in Fig. 2(a) are the fitting curves with Eq. (3). In the previous study [53], 1D diffusion model showed better consistency with the experimental data. The exact reason for that was not still very clear, but we strongly speculated that the diffusion coefficient of C excitons might be strongly anisotropic, which can allow effective diffusion only along one dimension in a MoS$_2$ monolayer.

On the basis of values of a and N_0 of MoS$_2$ monolayers, which are 3.16 Å and $5.7 \times 10^{14}\,cm^{-2}$, respectively, we extracted the values of D for each f_{pump} and plot them as a function of inverse square root of the pump fluence, $(f_{pump})^{-1/2}$ in Fig. 2(c). Since the temperature (T) induced by pump is proportional to f_{pump} the linear relationship between D and $(f_{pump})^{-1/2}$ indicates that D linearly increases with the inverse square root of temperature ($T^{-1/2}$) [62]. In the previous work, for free excitons where the exciton jumps before the lattice relaxes around the excited molecule, the relationship $D \sim T^{-1/2}$ was derived for the situation where the scattering by phonons is the dominant mechanism limiting the mean free path of the exciton [62]. Therefore, the linear behavior of D with $T^{-1/2}$ clearly indicates that the diffusion process of the C exciton takes place through exciton-phonon coupling. Figure 2(d) presents the annihilation rate with diffusion process, $\gamma_D(t)$, as a function of time delay [Eq. (2a)] for different pump fluences. The higher pump fluence, that is, the higher exciton density, the faster the annihilation rate.

V. FRET PROCESS: A AND B EXCITONS

Figure 3 presents the TA kinetics of A and B excitons in MoS$_2$ monolayer for the same pump fluences ($f_{pump} = 1, 5, 15, 25, 50\,\mu J\,cm^{-2}$) at 2.25 eV with probe energy of 1.85 and 2.01 eV, respectively. Ideally, A and B excitons should be measured resonantly as in the case for the C exciton. However, as the hot carrier relaxation in monolayer MoS$_2$ is much faster than the annihilation rate of excitons, we can neglect its contribution. The positive signal of ΔR for A and

TABLE I. Decay time constants of A, B, and C excitons for several pump fluences.

$f_{pump}(\mu J\,cm^{-2})$	A exciton		B exciton		C exciton	
	τ_1(ps)	τ_2(ps)	τ_1(ps)	τ_2(ps)	τ_1(ps)	τ_2(ps)
1	–	189	–	180	–	219
5	17.8	188	18.7	182	31.6	222
15	14.8	193	15.3	183	29.7	225
30	12.1	187	12.8	188	27.4	221
50	8.8	195	9.6	186	24.8	227

B excitons may be attributed to either a ground state bleach or stimulated emission of the pump-induced excited states. Similar to the C exciton, a single decay time (intrinsic exciton lifetimes) of 189 ps (181 ps) was obtained for the A (B) exciton at the lowest f_{pump}. Relatively short exciton lifetime in these band-edge excitons compared to C exciton is indeed consistent with previous work in which a longer lifetime of C excitons was reported owing to favorable band alignment and the transient excited state Coulomb environment [35]. In addition, as we mentioned earlier, no feature arising from the defect state was observed in photoluminescence and Raman spectra, which indicates that defect states should be nonradiative even if they can be excited at all. However, no other time constants responsible for possible defect states were observed at the lowest exciton density [black dots in Figs. 3(a) and 3(b)], which plainly means that defects do not play a significant role in this study.

We also notice that EEA comes into play for both A and B excitons as f_{pump} increases, giving rise to the emergence of short time constant (τ_1) (Table I). This fast decay component might be assigned to both exciton-exciton annihilations and trap states leading to the rapid relaxation [54]. It is worth noting that relatively slow trap-assisted recombination compared to intrinsic exciton recombination allows us to assume that the effect of trap state is presumably not very significant. Besides, we note that a previous study investigated the trap-assisted recombination of the MoS_2 monolayer and reported that the fast decay time became marginally faster (~10%) with increasing pump fluence up to $32\,\mu J\,cm^{-2}$ [63]. The current experimental result exhibiting more than 30% decrease in the fast decay time (see Table I at $30\,\mu J\,cm^{-2}$) thus indicates that fast decay is mainly attributed to EEA. The longer time constant (τ_2) that is independent of f_{pump} corresponds to the intrinsic exciton lifetime. It is worth noting that TA kinetics of A and B excitons exhibit stronger dependence on f_{pump} compared to the C exciton, which is consistent with the efficient dissociation of C exciton due to self-separation of photocarriers in the band nesting region.

In general, diffusion coefficient D for exciton annihilation may or may not be dependent on f_{pump}. In addition, the diffusion process can take place regardless of the emissivity of the exciton. On the other hand, the FRET occurs only when the exciton is emissive and is independent of f_{pump}. In this section, we discuss the FRET as a possible annihilation mechanism of A and B excitons. Similar to diffusion, the solution of Eq. (1) for FRET in 2D materials is given by [50]

$$n_F(t) = \frac{n_0 e^{-t/\tau}}{1 + \frac{n_0 R_F^2 \pi^2}{4} \text{erf}\left(\sqrt{\frac{t}{\tau}}\right)} \quad (4)$$

where the R_F is the Förster radius, the distance between donor and acceptor at which the energy transfer efficiency is 50%. R_F depends on the overlap integral of the donor emission spectrum with the acceptor absorption spectrum and their mutual orientation as expressed by the following equation [64]:

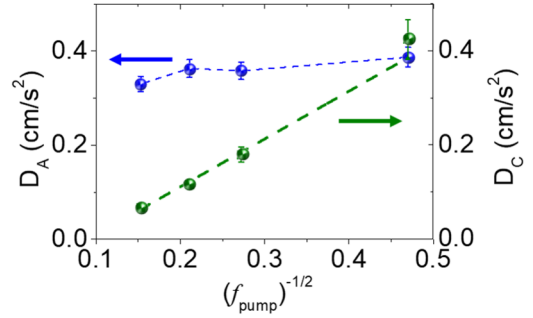$$R_F^6 = \frac{9\eta_D \kappa^2}{128\pi^5 n^4} \int d\lambda \lambda^4 F_D(\lambda)\sigma_A(\lambda), \quad (5)$$

FIG. 4. Plot of diffusion coefficient of the A exciton (D_A) and C exciton (D_C) as a function of inverse square root of the pump fluence.

where κ is the dipole orientation factor, n is the refraction index of the environment, λ is the wavelength, F_D is the normalized emission spectrum of donor, and σ_A is the absorption cross section of the acceptor. η_D is the quantum yield of the isolated donor expressed as the ratio of the rate of radiative recombination to the total rate of exciton decay. We note that η_D, F_D, and σ_A are the individual properties for isolated configuration so that the above equation is not associated with the density of donor and acceptor. The black solid lines in Figs. 3(a) and 3(b) are fitting curves based on Eq. (4), from which we extract the values of R_F.

First, let us assume that the A exciton annihilates via diffusion. According to a previous study [62], the temperature dependence of the diffusion coefficient for free excitons can be either proportional to $T^{-1/2}$ or constant depending on whether the temperature is above the Debye temperature (T_D) or not. In other words, D is constant for $T < T_D$ and has $T^{-1/2}$ dependence for $T > T_D$. Since we have already demonstrated that D_C represents $T^{-1/2}$ dependency [Fig. 2(c)], we can conclude that the temperature of the C exciton (T_C) is higher than T_D, ($T_C > T_D$). For the A exciton, we can also plot the D_A versus $(f_{pump})^{-1/2}$ under this assumption. As shown in Fig. 4, the constant behavior of D_A (blue), indicates that diffusion of the A exciton takes place via exciton-phonon coupling under $T_A < T_D$. Therefore, this analysis unambiguously shows that T_C is higher than T_A ($T_A < T_C$). However, the same f_{pump} for A and C excitons indicates $T_A = T_C$, which is obviously inconsistent with above result of $T_A < T_C$. Consequently, our assumption that the A exciton annihilates via the diffusion process is incorrect. Given the fact that there are only two mechanisms of exciton annihilation, FRET and diffusion, this systematic analysis, proving that the diffusion cannot be the annihilation mechanism of the A exciton, is very strong evidence for an underlying annihilation mechanism of the A exciton being a FRET, not a diffusion. In addition, previous studies have shown very weak temperature dependence of the Auger scattering process [65,66] that are related to the FRET rather than diffusion. This indicates that temperature independence of the A exciton compared to the C exciton also strongly supports the FRET as an annihilation mechanism of the A exciton.

Second, we extract R_F values of the A (B) exciton by fitting TA kinetics shown in [Figs. 3(a) and 3(b)] with Eq. (4) and plot it versus $(f_{pump})^{-1/2}$ in [Figs. 5(a) and 5(b)]. Constant behavior of R_F irrespective of f_{pump} indicates that R_F is not
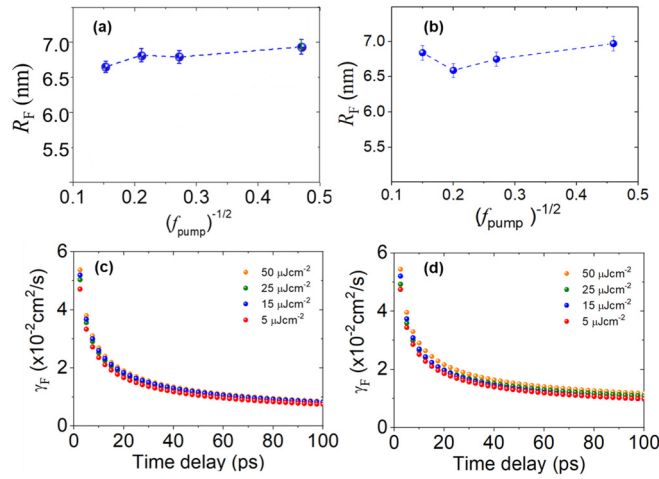
FIG. 5. (a), (b) Plot of Förster radius for A and B excitons as a function of inverse square root of the pump fluence, respectively. (c), (d) Plot of annihilation rate of A and B excitons via FRET as a function of time delay [Eq. (2b)], respectively.

dependent on the exciton density n_0 and temperature, which is consistent with basic nature of R_F represented by Eq. (5). In line with this, Figs. 5(c) and 5(d) also shows that the annihilation rate with FRET is almost independent of f_{pump}.

Third, we provide the evidence of FRET as an annihilation mechanism of A and B excitons by showing the spectral overlap between donor emission and acceptor absorption spectra. In case of homo-FRET, where the energy transfer occurs from the same entity, exciton emission, and ESA, are always overlapped as shown in Fig. 6(a). Efficient FRET can be expected for the annihilation step $E_1 + E_1 \rightarrow E_n + E_0$, with E_n being the final state in the TA experiments. Here, E_{10} is

the energy of radiative recombination, photoluminescence of the A exciton, and E_{12} is the energy of ESA from the first excited (exciton) state to second excited state. Depending on the pump energy, ESA can become E_{1n}, transition energy from the first excited (exciton) state to n^{th} excited state. In general, E_{10} is in between E_{12} and $E_{1n}(E_{12} < E_{10} < E_{1n})$, which was confirmed by previous work showing spectral overlap between the photoluminescence and the ESA of the A exciton [54]. Hence, this spectral overlap between E_{10} and E_{1n} is more critical evidence for FRET as an annihilation mechanism of the A exciton.

Finally, we corroborate the quenching of emission of the donor, or the reduction in lifetime of the donor due to its increased local density of optical states. We note that τ_1, responsible for EEA, is strongly associated with the quenched lifetime of the donor. In Fig. 6(b), a significant decrease in τ_1 with f_{pump} for the A exciton (Table I) is analogous to the decrease of donor exciton lifetime when FRET takes place. In order to understand more manifestly, we provide the schematic description of FRET between A excitons [Fig. 6(c)]. Upon photoexcitation, multiple excitons are generated, and FRET occurs in such a way that energy is transferred between two excitons as one of two excitons recombines, reflected in a decrease in the exciton lifetime $(\tau_1 < \tau_2)$. Energy transferred to another exciton leads to ESA, herein free carrier absorption in the conduction band. The hot electrons resulting from free carrier absorption eventually undergo intraband relaxation (usually the sub-ps time scale [33]) and interband relaxation (recombination of exciton, τ_2). In here, decrease in τ_1 manifestly shows the quenching effect of the donor exciton. We plot τ_1 of A, B, and C excitons altogether versus exciton density in Fig. 7 and find that the decreasing rate of τ_1 for the C exciton (21.6%) is relatively small compared with A and B excitons (~50%) (Table I).
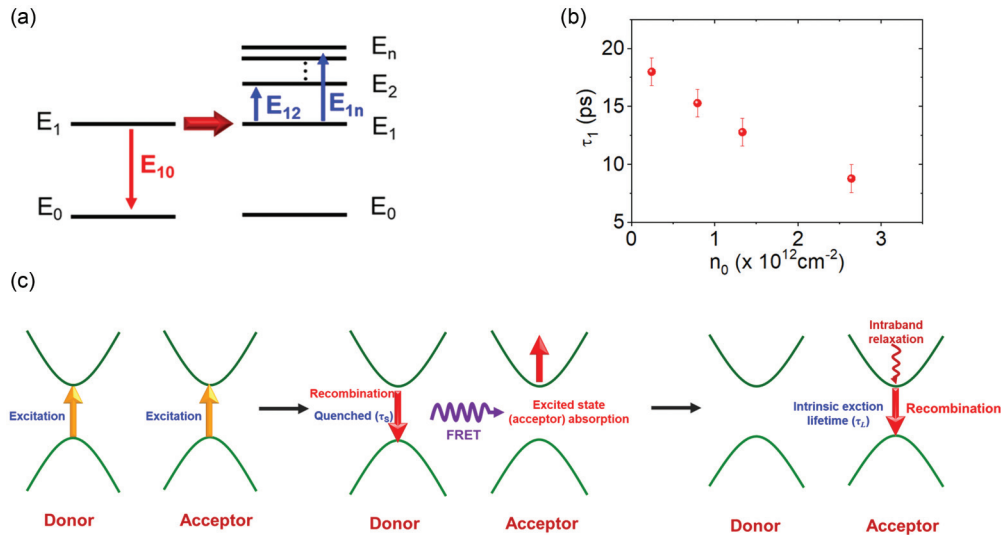

FIG. 6. (a) FRET process between identical excitons. Exciton annihilation between two identical molecules can be described via the FRET with a spectral overlap between the exciton emission (E_{10}) and the absorption of the exciton state to higher electronic states ($E_{12}, \ldots, E_{1n}$). (b) Fast decay time (τ_1) as a function of initial exciton density. (c) Schematic description of FRET between A excitons occurring in 2D MoS$_2$. Upon photoexcitation, multiple excitons can be generated simultaneously. Energy is transferred between two excitons as one of two excitons recombines nonradiatively, resulting in quenching of donor exciton (decrease of τ_1). Energy transferred to another exciton leads to free carrier absorption in the conduction band. The hot electrons undergo intraband or interband (τ_2) relaxation.
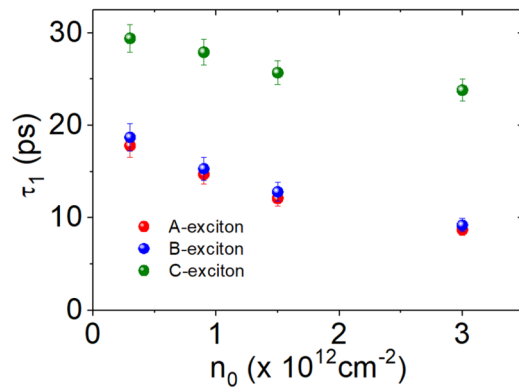
FIG. 7. Behavior of fast decay time component (τ_1) of A, B, and C excitons as a function of exciton density.

This indicates that EEA of A and B excitons occurs more actively than the C exciton. We attribute this to the fact that annihilation via direct interaction (FRET) leads to a faster decay process compared to annihilation via multiple interaction (Diffusion).

VI. DISCUSSION AND CONCLUSION

In this study, we have systematically studied the exciton annihilation mechanism in a MoS_2 monolayer based on the transient absorption spectroscopy. We observed the exciton-exciton annihilation of A, B, and C excitons and demonstrated that the multistep diffusion mediated by exciton-phonon scattering is responsible for C-exciton annihilation, while annihilation of A and B excitons is predominantly governed by direct FRET. We provided critical evidence to underpin the FRET as an annihilation mechanism of A and B excitons: exclusion of the diffusion process, independence of Förster radius to temperature and exciton density, and the donor quenching effect. We note that most of previous studies [39–44] have focused on the phenomenological effect of EEA by reporting the relatively fast EEA process in monolayer TMDs. In the current study, we concentrated on unraveling the underlying mechanism of the exciton annihilation mechanism for A, B, and C excitons based on the exact solutions of Eq. (1), given by Eqs. (3) and (4). The fact that FRET and diffusion processes as the main annihilation mechanisms for A, B, and C excitons, respectively, will provide a scientific basis for controlling exciton dynamics in 2D TMD materials. For example, we can control the EEA process of A and B excitons by changing the dielectric environment and applying the external field since FRET takes place via Coulomb interaction [53,67,68]. For the C exciton, there is a great demand for slowing down the C-exciton relaxation process because of ultrafast intraband relaxation within the sub-picosecond timescale, which is not beneficial to the efficient extraction of hot carriers and restricts the upper limit of the quantum yield of TMDs-based light-harvesting devices. A recent study has reported relatively slow cooling of the C exciton (tens of picosecond) due to the intervalley transfer process (Ref. [36]). This indicates that the diffusion process of C-exciton annihilation can be controlled by means of bandgap engineering such as photoinduced bandgap renormalization [69], plasmonic excitation [70], and chemical treatment [71]. Given that a comprehensive understanding of excitonic properties of monolayer MoS_2 is crucial for various applications in photonics and optoelectronics, unraveling the underlying mechanism of exciton annihilation for each type of exciton in the MoS_2 monolayer presented in this study will offer insights on the excitonic properties of 2D TMDs.

[1] G. R. Bhimanapati, Z. Lin, V. Meunier, Y. Jung, J. Cha, S. Das, D. Xiao, Y. Son, M. S. Strano, V. R. Cooper, L. Liang, S. G. Louie, E. Ringe, W. Zhou, S. S. Kim, R. R. Naik, B. G. Sumpter, H. Terrones, F. Xia, Y. Wang, J. Zhu, D. Akinwande, N. Alem, J. A. Schuller, R. E. Schaak, M. Terrones, and J. A. Robinson, ACS Nano **9**, 11509 (2015).

[2] S. Das, J. A. Robinson, M. Dubey, H. Terrones, and M. Terrones, Annu. Rev. Mater. Res. **45**, 1 (2015).

[3] G. Eda and S. A. Maier, ACS Nano **7**, 5660 (2013).

[4] S. Z. Butler, S. M. Hollen, L. Cao, Y. Cui, J. A. Gupta, H. R. Gutiérrez, T. F. Heinz, S. S. Hong, J. Huang, A. F. Ismach, E. Johnston-Halperin, M. Kuno, V. V. Plashnitsa, R. D. Robinson, R. S. Ruoff, S. Salahuddin, J. Shan, L. Shi, M. G. Spencer, M. Terrones, W. Windl, and J. E. Goldberger, ACS Nano **7**, 2898 (2013).

[5] Z. Hu, Z. Wu, C. Han, J. He, Z. Ni, and W. Chen, Chem. Soc. Rev. **47**, 3100 (2018).

[6] K. F. Mak, D. Xiao, and J. Shan, Nat. Photonics **12**, 451 (2018).

[7] X. Duan, C. Wang, A. Pan, R. Yu, and X. Duan, Chem. Soc. Rev. **44**, 8859 (2015).

[8] S. Manzeli, D. Ovchinnikov, D. Pasquier, O. V. Yazyev, and A. Kis, Nat. Rev. Mater. **2**, 17033 (2017).

[9] B. Radisavljevic, A. Radenovic, J. Brivio, V. Giacometti, and A. Kis, Nat. Nanotechnol. **6**, 147 (2011).

[10] J. Lu, H. Liu, E. S. Tok, and C. H. Sow, Chem. Soc. Rev. **45**, 2494 (2016).

[11] T. Cao, G. Wang, W. Han, H. Ye, C. Zhu, J. Shi, Q. Niu, P. Tan, E. Wang, B. Liu, and J. Feng, Nat. Commun. **3**, 887 (2012).

[12] D. Xiao, G. B. Liu, W. Feng, X. Xu, and W. Yao, Phys. Rev. Lett. **108**, 196802 (2012).

[13] L. Sun, C.-Y. Wang, A. Krasnok, J. Choi, J. Shi, J. S. Gomez-Diaz, A. Zepeda, S. Gwo, C.-K. Shih, A. Alù, and X. Li, Nat. Photonics **13**, 180 (2019).

[14] Z. Sun, J. Gu, A. Ghazaryan, Z. Shotan, C. R. Considine, M. Dollar, B. Chakraborty, X. Liu, P. Ghaemi, S. Kéna-Cohen, and V. M. Menon, Nat. Photonics **11**, 491 (2017).

[15] K. F. Mak, K. He, J. Shan, and T. F. Heinz, Nat. Nanotechnol. **7**, 494 (2012).

[16] S. Jo, N. Ubrig, H. Berger, A. B. Kuzmenko, and A. F. Morpurgo, Nano Lett. **14**, 2019 (2014).

[17] Z. Yin, H. Li, H. Li, L. Jiang, Y. Shi, Y. Sun, G. Lu, Q. Zhang, X. Chen, and H. Zhang, ACS Nano **6**, 74 (2012).

[18] J. Kwon, Y. K. Hong, G. Han, I. Omkaram, W. Choi, S. Kim, and Y. Yoon, Adv. Mater. **27**, 2224 (2015).

[19] C. Xie, C. Mak, X. Tao, and F. Yan, Adv. Funct. Mater. **27**, 1603886 (2017).

[20] L. Britnell, R. M. Ribeiro, A. Eckmann, R. Jalil, B. D. Belle, A. Mishchenko, Y. Kim, R. V. Gorbachev, T. Georgiou, S. V. Morozov, A. N. Grigorenko, A. K. Geim, C. Casiraghi, A. H. C. Neto, and K. S. Novoselov, Science **340**, 1311 (2013).

[21] N. Perea-Lõpez, A. L. Elías, A. Berkdemir, A. Castro-Beltran, H. R. Gutiérrez, S. Feng, R. Lv, T. Hayashi, F. Lõpez-Urías, S. Ghosh, B. Muchharla, S. Talapatra, H. Terrones, and M. Terrones, Adv. Funct. Mater. **23**, 5511 (2013).

[22] F. K. Perkins, A. L. Friedman, E. Cobas, P. M. Campbell, G. G. Jernigan, and B. T. Jonker, Nano Lett. **13**, 668 (2013).

[23] J. R. Schaibley, H. Yu, G. Clark, P. Rivera, J. S. Ross, K. L. Seyler, W. Yao, and X. Xu, Nat. Rev. Mater. **1**, 1 (2016).

[24] J. Kim, C. Jin, B. Chen, H. Cai, T. Zhao, P. Lee, S. Kahn, K. Watanabe, T. Taniguchi, S. Tongay, M. F. Crommie, and F. Wang, Sci. Adv. **3**, e1700518 (2017).

[25] Y. J. Chen, J. D. Cain, T. K. Stanev, V. P. Dravid, and N. P. Stern, Nat. Photonics **11**, 431 (2017).

[26] K. F. Mak, C. Lee, J. Hone, J. Shan, and T. F. Heinz, Phys. Rev. Lett. **105**, 136805 (2010).

[27] K. He, N. Kumar, L. Zhao, Z. Wang, K. F. Mak, H. Zhao, and J. Shan, Phys. Rev. Lett. **113**, 026803 (2014).

[28] M. M. Ugeda, A. J. Bradley, S. F. Shi, F. H. Da Jornada, Y. Zhang, D. Y. Qiu, W. Ruan, S. K. Mo, Z. Hussain, Z. X. Shen, F. Wang, S. G. Louie, and M. F. Crommie, Nat. Mater. **13**, 1091 (2014).

[29] A. Chernikov, T. C. Berkelbach, H. M. Hill, A. Rigosi, Y. Li, O. B. Aslan, D. R. Reichman, M. S. Hybertsen, and T. F. Heinz, Phys. Rev. Lett. **113**, 076802 (2014).

[30] A. Splendiani, L. Sun, Y. Zhang, T. Li, J. Kim, C. Y. Chim, G. Galli, and F. Wang, Nano Lett. **10**, 1271 (2010).

[31] S. Sim, J. Park, J. G. Song, C. In, Y. S. Lee, H. Kim, and H. Choi, Phys. Rev. B **88**, 075434 (2013).

[32] A. Carvalho, R. M. Ribeiro, and A. H. Castro Neto, Phys. Rev. B **88**, 115205 (2013).

[33] D. Kozawa, R. Kumar, A. Carvalho, K. Kumar Amara, W. Zhao, S. Wang, M. Toh, R. M. Ribeiro, A. H. Castro Neto, K. Matsuda, and G. Eda, Nat. Commun. **5**, 4543 (2014).

[34] A. R. Klots, A. K. M. Newaz, B. Wang, D. Prasai, H. Krzyzanowska, J. Lin, D. Caudel, N. J. Ghimire, J. Yan, B. L. Ivanov, K. A. Velizhanin, A. Burger, D. G. Mandrus, N. H. Tolk, S. T. Pantelides, and K. I. Bolotin, Sci. Rep. **4**, 6608 (2014).

[35] L. Wang, Z. Wang, H. Wang, G. Grinblat, Y. Huang, D. Wang, X. Ye, X. Li, Q. Bao, A. Wee, S. A. Maier, Q. Chen, and M. Zhong, Nat. Commun. **8**, 13906 (2017).

[36] Y. Li, J. Shi, H. Chen, Y. Mi, W. Du, X. Sui, C. Jiang, W. Liu, H. Xu, and X. Liu, Laser Photonics Rev. **13**, 1800270 (2019).

[37] F. Withers, O. Del Pozo-Zamudio, A. Mishchenko, A. P. Rooney, A. Gholinia, K. Watanabe, T. Taniguchi, S. J. Haigh,

A. K. Geim, A. I. Tartakovskii, and K. S. Novoselov, Nat. Mater. **14**, 301 (2015).

[38] O. Lopez-Sanchez, E. Alarcon Llado, V. Koman, A. Fontcuberta I Morral, A. Radenovic, and A. Kis, ACS Nano **8**, 3042 (2014).

[39] D. Sun, Y. Rao, G. A. Reider, G. Chen, Y. You, L. Brézin, A. R. Harutyunyan, and T. F. Heinz, Nano Lett. **14**, 5625 (2014).

[40] N. Kumar, Q. Cui, F. Ceballos, D. He, Y. Wang, and H. Zhao, Phys. Rev. B **89**, 125427 (2014).

[41] L. Yuan and L. Huang, Nanoscale **7**, 7402 (2015).

[42] G. Froehlicher, E. Lorchat, and S. Berciaud, Phys. Rev. B **94**, 085429 (2016).

[43] A. Surrente, A. A. Mitioglu, K. Galkowski, L. Klopotowski, W. Tabis, B. Vignolle, D. K. Maude, and P. Plochocka, Phys. Rev. B **94**, 075425 (2016).

[44] Y. Yu, Y. Yu, C. Xu, A. Barrette, K. Gundogdu, and L. Cao, Phys. Rev. B **93**, 201111(R) (2016).

[45] K. Feron, X. Zhou, W. J. Belcher, and P. C. Dastoor, J. Appl. Phys. **111**, 044510 (2012).

[46] F. Fennel and S. Lochbrunner, Phys. Rev. B **92**, 140301(R) (2015).

[47] E. Engel, K. Leo, and M. Hoffmann, Chem. Phys. **325**, 170 (2006).

[48] S. F. Völker, A. Schmiedel, M. Holzapfel, K. Renziehausen, V. Engel, and C. Lambert, J. Phys. Chem. C **118**, 17467 (2014).

[49] O. V. Mikhnenko, P. W. M. Blom, and T. Q. Nguyen, Energy Environ. Sci. **8**, 1867 (2015).

[50] Y. Zaushitsyn, K. G. Jespersen, L. Valkunas, V. Sundström, and A. Yartsev, Phys. Rev. B **75**, 195201 (2007).

[51] Y. Tamai, H. Ohkita, H. Benten, and S. Ito, J. Phys. Chem. Lett. **6**, 3417 (2015).

[52] H.-Y. Shin, J. H. Woo, M. J. Gwon, M. Barthelemy, M. Vomir, T. Muto, K. Takaishi, M. Uchiyama, D. Hashizume, T. Aoyama, D.-W. Kim, S. Yoon, J.-Y. Bigot, J. W. Wu, and J. C. Ribierre, Phys. Chem. Chem. Phys. **15**, 2867 (2013).

[53] K. J. Lee, W. Xin, C. Fann, X. Ma, F. Xing, J. Liu, J. Zhang, M. Elkabbash, and C. Guo, Phys. Rev. B **101**, 041405(R) (2020).

[54] S. H. Aleithan, M. Y. Livshits, S. Khadka, J. J. Rack, M. E. Kordesch, and E. Stinaff, Phys. Rev. B **94**, 035445 (2016).

[55] C. Ruckebusch, M. Sliwa, P. Pernot, A. de Juan, and R. Tauler, J. Photochem. Photobiol. C Photochem. Rev. **13**, 1 (2012).

[56] H. Ohkita, S. Cook, Y. Astuti, W. Duffy, S. Tierney, W. Zhang, M. Heeney, I. McCulloch, J. Nelson, D. D. C. Bradley, and J. R. Durrant, J. Am. Chem. Soc. **130**, 3030 (2008).

[57] K. J. Lee, Y. Xiao, J. H. Woo, E. Kim, D. Kreher, A. J. Attias, F. Mathevet, J. C. Ribierre, J. W. Wu, and P. André, Nat. Mater. **16**, 722 (2017).

[58] K. J. Lee, Y. Xiao, E. S. Kim, F. Mathevet, L. Mager, O. Cregut, F. Fages, J. C. Ribierre, J. W. Wu, and A. D'Aléo, ACS Photonics **6**, 2649 (2019).

[59] R. Berera, R. van Grondelle, and J. T. M. Kennis, Photosynth. Res. **101**, 105 (2009).

[60] K. J. Lee, J. H. Woo, Y. Xiao, E. Kim, L. M. Mazur, D. Kreher, A. J. Attias, K. Matczyszyn, M. Samoc, B. Heinrich, S. Méry, F. Fages, L. Mager, A. D'Aléo, J. W. Wu, F. Mathevet, P. André, and J. C. Ribierre, RSC Adv. **6**, 57811 (2016).

[61] M. Brendel, A. Kruse, H. Jönen, L. Hoffmann, H. Bremers, U. Rossow, and A. Hangleiter, Appl. Phys. Lett. **99**, 031106 (2011).

[62] R. C. Powell and Z. G. Soos, Phys. Rev. B **5**, 1547 (1972).

[63] H. Wang, C. Zhang, and F. Rana, Nano Lett. **15**, 339 (2015).

[64] T. Förster, Ann. Phys. **437**, 55 (1948).

[65] G. M. Kavoulakis and G. Baym, Phys. Rev. B **54**, 16625 (1996).

[66] F. Wang, Y. Wu, M. S. Hybertsen, and T. F. Heinz, Phys. Rev. B **73**, 245424 (2006).

[67] V. N. Peters, S. Prayakarao, S. R. Koutsares, C. E. Bonner, and M. A. Noginov, ACS Photonics **6**, 3039 (2019).

[68] A. Raja, A. Chaves, J. Yu, G. Arefe, H. M. Hill, A. F. Rigosi, T. C. Berkelbach, P. Nagler, C. Schüller, T. Korn, C. Nuckolls, J. Hone, L. E. Brus, T. F. Heinz, D. R. Reichman, and A. Chernikov, Nat. Commun. **8**, 15251 (2017).

[69] P. D. Cunningham, A. T. Hanbicki, K. M. McCreary, and B. T. Jonker, ACS Nano **11**, 12601 (2017).

[70] Z. Li, Y. Xiao, Y. Gong, Z. Wang, Y. Kang, S. Zu, P. M. Ajayan, P. Nordlander, and Z. Fang, ACS Nano **9**, 10158 (2015).

[71] A. J. Goodman, A. P. Willard, and W. A. Tisdale, Phys. Rev. B **96**, 121404(R) (2017).